Lattice-distortion effects on the magnetism of Mn impurities in Al and Cu

Diana Guenzburger
Centro Brasileiro de Pesquisas Físicas, Rua Dr. Xavier Sigaud, 150, 22290-180 Rio de Janeiro, RJ, Brazil

D. E. Ellis
Northwestern University, Evanston, Illinois 60208
and Centro Brasileiro de Pesquisas Físicas, Rua Dr. Xavier Sigaud, 150, 22290-180 Rio de Janeiro, RJ, Brazil
(Received 20 September 1993)

Self-consistent calculations with the discrete variational method in the framework of local spin-density theory were performed for 43-atom embedded clusters representing a Mn impurity in Al and Cu hosts. Effects of local lattice relaxation were explored by varying the distance between Mn and the nearest-neighbor host atoms. It was found that the magnetic moment of Mn in Al is much more sensitive to local lattice distortion than Mn in Cu. At the equilibrium Mn nearest-neighbors distance, as determined by x-ray absorption fine-structure measurements, a reduction of 34% of μ in Al is obtained, relative to the host lattice distance. Mechanisms related to the effect of the environment on μ are discussed. The Mn 3*s* exchange splitting observed in x-ray photoelectron spectra is also investigated, and it is found that it may not be taken as evidence of a 3*d* moment in the ground state.

I. INTRODUCTION

The existence of local magnetism on transition-element impurities in metal hosts has been the subject of much experimental and theoretical work.[1,2] In many cases, however, the question of whether and why an impurity in a metallic system possesses a stable moment has not been answered to satisfaction. To understand an impurity-host system, one must take into account the effects of the local environment on the solute atoms. The atomic neighbors in the host interact with the impurity by hybridization with impurity orbitals, and some charge transfer will take place. Other effects are also present, caused by local adaptation of the atomic positions of the neighbors to the different atomic volume of the solute atom; in addition, electronic charge on the impurity may be compressed or extended to adapt to the host, due to the Pauli exclusion principle. All these mechanisms will be reflected in the magnetism of the impurity and may be investigated through electronic structure calculations.[3,4]

We report a study of the effect of the local environment on the magnetism of a Mn impurity in two different hosts, Al and Cu. Both have fcc structure; however, the magnetic behavior of Mn in these metals may be quite different. There is ample evidence that a Mn impurity in Cu has a quite stable magnetic moment; in fact, resistivity measurements of dilute alloys,[2] as well as thermopower,[5] susceptibility,[5,6] and, more recently, time-differential perturbed γ-ray angular distribution (TDPAD) measurements of the implanted ion,[7] all point to a large and stable spin moment on Mn. On the other hand, the situation regarding dilute alloys of Mn in Al is more controversial. Magnetization measurements indicate no local magnetism of the Mn impurity in both solid[8] and liquid[9] Al, since the susceptibility does not follow a Curie-Weiss law. The different behavior of the resistivity of first-row transition-metal impurities in Al and Cu hosts may be explained within a Friedel-Anderson model if the impurity-host systems are assumed to be nonmagnetic for the former and magnetic for the latter.[2] On the other hand, neutron-diffraction studies show evidence for the existence of a magnetic moment on Mn in Al, which is compensated at low temperatures by an antiferromagnetic cloud of estimated 5–6 Å radius.[10,11] Furthermore, x-ray photoelectron spectra (XPS) of Mn in Al present a splitting of the 3*s* level of Mn that was interpreted as originating from the exchange interaction with a 3*d* moment in the ground state.[12]

We employed the discrete variational method[13] and local spin-density theory[14] to obtain the electronic structure of 43-atom embedded clusters, representing a Mn impurity in the hosts Cu and Al. In addition to the influence of the different metal hosts on the magnetism of the impurity, lattice-distortion effects were explored by allowing the distance between Mn and the first shell of host neighbor atoms to vary. A previously reported study of an Fe impurity in an Al host has shown that local lattice relaxation has a strong effect in quenching the theoretically obtained magnetic moment on Fe.[3,4] We also investigate the possible mechanisms leading to the observed magnetic behavior of the impurity-host systems. The exchange splitting of the Mn 3*s* level is also investigated.

This paper is organized as follows. In Sec. II we briefly describe the theoretical method, in Sec. III we discuss the magnetism of the impurity-host systems in the ground state, in Sec. IV we discuss the XPS 3*s*-level splitting, and in Sec. V we summarize our conclusions.

II. THEORETICAL METHOD

The method employed was the discrete variation (DV) method, which has been described in detail in the literature.[13,15] Here we give a summary of the main features

 ©1994 The American Physical Society

relevant to the present work. The DV method is based on local spin-density theory in which the energy is a functional of the electronic density ρ_σ,

$$\rho_\sigma(\mathbf{r})=\sum_i n_{i\sigma}|\phi_{i\sigma}(\mathbf{r})|^2 \quad (1)$$

for each spin σ. In the present spin-polarized calculations, ρ_σ has the freedom to be different for each spin σ. $n_{i\sigma}$ is the occupation of the cluster spin-orbital $\phi_{i\sigma}$, defined as a linear combination of numerical symmetrized atomic orbitals χ_j^s (LCAO),

$$\phi_{i\sigma}(\mathbf{r})=\sum_j \chi_j^s(\mathbf{r})C_{ji}^\sigma \ . \quad (2)$$

$\{\phi_{i\sigma}\}$ are the eigenvectors of the Kohn-Sham[14] equations (in hartrees),

$$(h_\sigma-\varepsilon_{i\sigma})\phi_{i\sigma}=(-\nabla^2/2+V_c+V_{xc}^\sigma-\varepsilon_{i\sigma})\phi_{i\sigma}=0 \ , \quad (3)$$

which are solved self-consistently in a three-dimensional numerical grid. In Eq. (3), V_c includes the nuclear and electronic Coulomb potentials and V_{xc}^σ is the exchange-correlation potential as derived by von Barth and Hedin.[16]

The variational procedure leads to the secular equations

$$([H]-[E][S])[C]=0 \ , \quad (4)$$

where $[H]$ is the matrix of the Kohn-Sham Hamiltonian, $[S]$ the overlap matrix, and $[C]$ the matrix of the eigenvectors. The elements of the $[H]$ and $[S]$ matrices are defined numerically in the three-dimensional grid.

The cluster orbitals are filled according to Fermi-Dirac statistics, with a "thermal smearing" around the Fermi level to assure convergence. The cluster charge is constrained to be zero; no constraint is posed on the spin magnetic moment. The cluster is embedded in the charge density of several shells of neighbor atoms in the lattice, obtained by self-consistent numerical local spin-density atomic calculations. The core region of the external potentials is truncated to simulate effects of the Pauli exclusion principle.[17]

A Mulliken-type population analysis[18] is performed, which is based on the coefficients of the LCAO expansion. Spin magnetic moments are thus defined as the difference between spin-up and spin-down populations on a given atom. The basis functions are improved by generating self-consistent-field (SCF) atomic orbitals for a configuration similar to that in the solid, as defined by the Mulliken populations.

Mulliken populations are also employed to define a partial density of states (DOS),

$$D_{nl\sigma}^q(E)=\sum_i P_{nl\sigma,i}^q \frac{\delta/\pi}{(E-\varepsilon_{i\sigma})^2+\delta^2} \ , \quad (5)$$

where $P_{nl\sigma,i}^q$ is the Mulliken-type population of atomic orbital χ_{nl} of atom q in the cluster spin orbital $\phi_{i\sigma}$. The cluster levels are broadened by Lorentzians with a convenient half-width δ to simulate the DOS diagrams obtained for a continuum of levels of an infinite solid. The total DOS is then, for spin σ,

$$D_\sigma(E)=\sum_{q,n,l} D_{nl\sigma}^q(E) \ . \quad (6)$$

To surmount the difficulties of calculating the Coulomb potential in a three-dimensional grid, the exact charge density obtained in each iteration is fitted to a model charge density,[19]

$$\rho(\mathbf{r})\cong\rho^M(\mathbf{r})=\sum_{n,l,I} d_{nl}^I \sum_q{}' |R_{nl}^q(r_q)|^2 Y_0^0(\hat{r}_q) \ , \quad (7)$$

where R_{nl}^q are the radial atomic functions of the basis and the prime in the second summation stands for a particular set of atoms q ($q\in I$) equivalent by symmetry. The coefficients are determined in each cycle by a least-squares fit to the true density, subject to the constraint that $\rho^M(\mathbf{r})$ integrates to the total number of electrons in the cluster. This model charge density is thus a superposition of overlapping spherical densities; expansion in higher multipoles is also possible within the DV method,[19] but less necessary for compact metals, where overlapping spherical densities are expected to be a good approximation to the true density.

III. ELECTRONIC STRUCTURE AND MAGNETIC MOMENTS

The clusters representing a Mn impurity in the fcc lattices of Al and Cu have the Mn atom placed at the center, 12 atoms of the host in the nearest-neighbor (NN) shell, 6 atoms as next-nearest-neighbors (NNN), and 24 atoms in the outermost shell. Figure 1 is a representation of the clusters. Both clusters are embedded in the potential of several shells of atoms of the respective hosts.

Initially, we performed self-consistent calculations for $[MnAl_{42}]$ and $[MnCu_{42}]$ at the host lattice equilibrium Mn-NN interatomic distances (2.86 Å for Al and 2.55 Å for Cu). The values obtained for the total $(3d+4s+4p)$ spin magnetic moment μ on Mn were $2.91\mu_B$ in Al and 3.81 in Cu.

Previously reported theoretical calculations, performed at the host interatomic distances, gave a value of $1.74\mu_B$

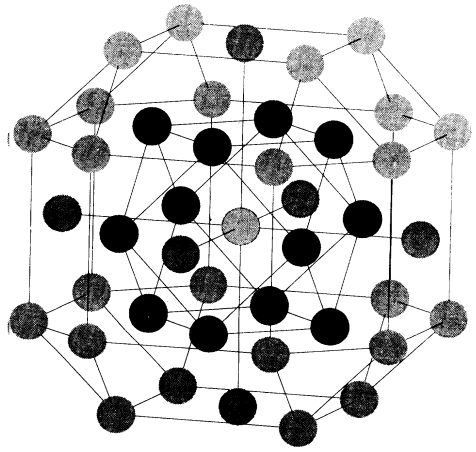

FIG. 1. View of the 43-atom cluster representing a Mn impurity in fcc Al and Cu. Darker spheres are atoms in the first shell of neighbors surrounding the central Mn.

for the magnetic moment μ of Mn in Al, as obtained in a 19-atom cluster calculation within local spin-density theory, employing Gaussian basis functions,[20] and $\mu=2.46\mu_B$ in another local spin-density calculation with an approximate treatment for the host.[21] A Mn impurity in Al was also calculated by the Green's-functions Korringa-Kohn-Rostoker (KKR) method, and a value $\mu(\text{Mn})=2.53\mu_B$ was obtained.[22] This latter method was also employed to calculate the electronic structure of a Mn impurity in Cu, giving $\mu(\text{Mn})=3.44\mu_B$.[23] It may be seen that our values at the host lattice interatomic distances do not differ substantially from those obtained with the Green's-functions method, the latter being somewhat lower. Recently, a calculation for Mn in Al with the DV method was reported;[24] the value obtained for μ(Mn) was $3.26\mu_B$. The small difference between this value of μ and the value reported here may be ascribed to differences in the basis functions, in the local exchange potential employed, in the model ρ, etc.

Since Al has a considerably larger lattice constant than Cu (4.05 and 3.61 Å, respectively), it may be expected that local volume effects around Mn will be different in the two metal hosts. To investigate the effect of the adaptation of atomic positions of neighbor atoms on the magnetism of Mn, we performed self-consistent-field calculations for clusters in which the Mn-NN distance was varied. The positions of the atoms in the NNN and outermost shells were maintained as in the host lattices. For $[MnAl_{42}]$, only Mn-Al(NN) distances smaller than the interatomic distances in Al were considered, since a compression was likely to occur; for $[MnCu_{42}]$, smaller and larger distances were investigated.

Figures 2 and 3 show the change in the Mn magnetic moment brought in by relaxation of the first shell of neighbors for $[MnAl_{42}]$ and $[MnCu_{42}]$, respectively. It may be observed that the effect of compression of the first

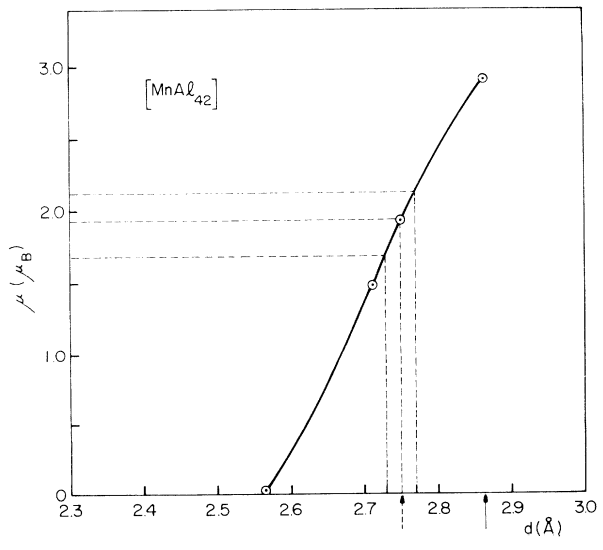

FIG. 2. Variation of total ($3d+4s+4p$) magnetic moment μ on Mn with Mn-NN distance in $[MnAl_{42}]$. Solid arrow marks the interatomic distance in the Al lattice; dotted arrow marks the Mn-NN distance as determined by XAFS.

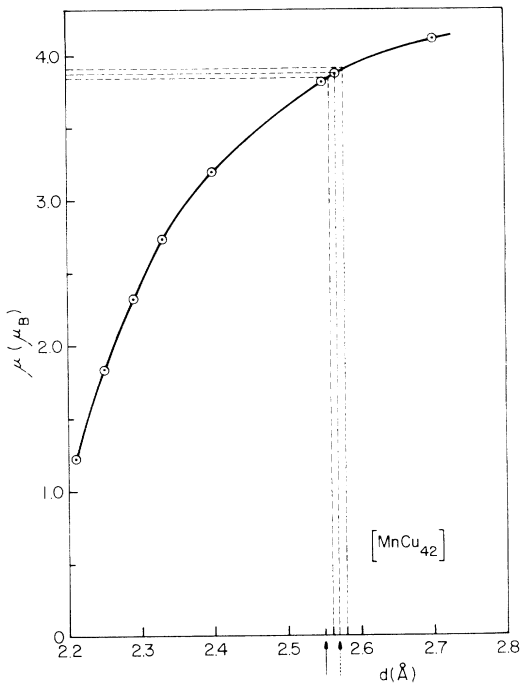

FIG. 3. Variation of total ($3d+4s+4d$) magnetic moment μ on Mn with Mn-NN distance in $[MnCl_{42}]$. Solid arrow marks the interatomic distance in the Cu lattice; dotted arrow marks the Mn-NN distance as determined by XAFS.

shell of neighbors on μ is much more drastic for Mn in Al than for Mn in Cu. In the former case, the Mn moment vanishes completely at $d(\text{Mn-NN})\cong 2.55$ Å, whereas for Mn in Cu, a rather large moment is still present at $d\sim 2.2$ Å. In fact, near the equilibrium lattice distance, a compression of 0.1 Å in d(Mn-NN) will bring about a decrease in μ(Mn) of $\sim 0.9\mu_B$ in $[MnAl_{42}]$ and of only $\sim 0.4\mu_B$ in $[MnCu_{42}]$. A similar variation of μ(Mn) was found in a calculation of Mn in Cu with the Green's-function method,[25] where it was concluded that the impurity moment in *Cu*Mn is rather insensitive to the displacement of the first neighbors. No analogous calculations are available for *Al*Mn, for which, as shown here, the effect is much more significant.

In a previous investigation of *Al*Fe, we have performed total-energy calculations at several Fe-NN distances to attempt to obtain the equilibrium interatomic distance by energy minimization and thus the equilibrium magnetic moment.[3] However, interatomic distances obtained in this manner are subject to errors. The main sources of errors are the following: Only the first shell of neighbors is displaced; the finite number of atoms in the cluster leads to deviations in calculated equilibrium distances from the values in the crystal; and the local density approximation induces errors in the determination of interatomic distances in metals,[26,27] the calculated values being usually shorter than those experimentally determined. A much more satisfactory procedure is to combine, when available, local distances determined by x-ray absorption fine-structure (XAFS) experiments with the calculations of magnetic moments. Such measurements have indeed been recently reported for Mn in Al and Mn

in Cu.[28] A very large reduction of the Mn-NN distance is found for Mn impurities in Al, giving a value of 2.75±0.02 Å. Considering the error bar reported, this places the magnetic moment on Mn anywhere in the interval $(1.68-2.12)\mu_B$ (see Fig. 2), a substantial decrease from the value $2.91\mu_B$ obtained at the Al lattice distance.

On the other hand, relaxation of Mn neighbors in Cu is found to be much smaller. We chose the value for the XAFS model system with the smallest error bar, which gives d(Mn-NN)=2.57±0.01 Å, a slight expansion relative to the Cu equilibrium value of 2.55 Å. For the expanded distance, we find μ(Mn)$=(3.85-3.91)\mu_B$ (see Fig. 3), a small increase from the value $3.81\mu_B$ for the Cu lattice distance. Some experimentally derived values of μ are $4.0\mu_B$ as obtained by magnetization measurements,[6] $3.5\mu_B$ by neutron scattering,[29] and $3.4\mu_B$ in a de Haas–van Alphen experiment.[30]

Thus we conclude that, by a combination of small volume expansion and low sensitivity of the local moment to neighbor displacements, relaxation is indeed unimportant for the magnetism of a Mn impurity in Cu. The opposite is the case for *Al*Mn, where the Al neighbor atoms are strongly compressed around the Mn impurity, and the steep dependence of μ with the Mn-NN distance results in a significant reduction of magnetism.

In Table I are displayed the values obtained for the Mulliken populations, charges, and magnetic moments for [$MnAl_{42}$] and [$MnCu_{42}$] for the calculations performed at the Mn-NN equilibrium interatomic distances according to XAFS measurements (2.75 and 2.57 Å, respectively). Mn has a negative charge in the Al host and positive in Cu. The positive charge on Mn in *Cu*Mn can be rationalized in terms of Pauling electronegativities Al(1.5)≅Mn(1.5)<Cu(1.8). However, the negative charge in *Al*Mn appears to be due to the extensive hybridization with Al 3p, the same interaction which sharply reduces the moment. From the Mulliken-type populations, it may be seen that it is mainly the Mn(3d) orbital that is depleted in the Cu host relative to Al. In the Cu host, the positive charge of Mn extends to the first two shells of neighbors, being compensated only in the outermost shell. In Al, the charge oscillates to positive in the NN and NNN shells and back to negative in the last. The 3s and 3p orbitals of Al have similar (and large) populations, whereas in Cu the 4s orbitals have larger occupations than the 4p. The Cu 3d electrons have a small but significant participation in bonding, as may be seen from the populations and magnetic moments of this orbital in all three shells of neighbors.

Small antiferromagnetically coupled spin moments appear in the surrounding NN host atoms, being much larger in Al than in Cu. In Al, the moments oscillate to ferromagnetic in the NNN shell and back to antiferromagnetic in the outermost shell. In Cu, the coupling turns to ferromagnetic in the NNN and outermost shells. The coupling between μ(Mn) and μ(3d Cu) is ferromagnetic in all shells. The coupling between the Mn 3d and (4s,4p) moments is ferromagnetic in both cases.

In Figs. 4 and 5 are depicted the changes with the Mn-NN distance in the Mn 3d populations associated with both spins for [$MnAl_{42}$] and [$MnCu_{42}$], respectively. It is seen that, in both cases, the decrease of μ(Mn) by

TABLE I. Electronic populations, charges, and magnetic moments μ (in μ_B) for [$MnAl_{12}Al_6Al_{24}$] and [$MnCu_{12}Cu_6Cu_{24}$] at the Mn-NN equilibrium distance (2.75 and 2.57 Å, respectively). Host atoms are numbered according to distance of the shell from Mn. Inner orbitals 3s and 3p of Mn, not shown in the table, present small deviations of populations relative to free atom values.

		[$MnAl_{42}$] Populations	μ			[$MnCu_{42}$] Populations	μ
Mn	3d	6.594	1.822	Mn	3d	5.802	3.665
	4s	0.520	0.054		4s	0.485	0.109
	4p	0.343	0.045		4p	0.322	0.103
Al(I)	3s	1.414	−0.004	Cu(I)	3d	9.830	0.020
	3p	1.553	−0.030		4s	0.723	−0.021
					4p	0.393	−0.017
Al(II)	3s	1.451	−0.011				
	3p	1.492	0.015	Cu(II)	3d	9.850	0.006
					4s	0.709	0.003
Al(III)	3s	1.681	−0.004		4p	0.329	−0.004
	3p	1.333	−0.001				
				Cu(III)	3d	9.835	0.004
					4s	0.921	0.002
					4p	0.319	−0.004
		Charge	Total μ			Charge	Total μ
Mn		−0.404	1.921	Mn		+0.463	3.877
Al(I)		+0.033	−0.034	Cu(I)		+0.054	−0.018
Al(II)		+0.057	+0.004	Cu(II)		+0.112	+0.005
Al(III)		−0.014	−0.005	Cu(III)		−0.075	+0.002
Total cluster		0.0	1.42	Total		0.0	3.74

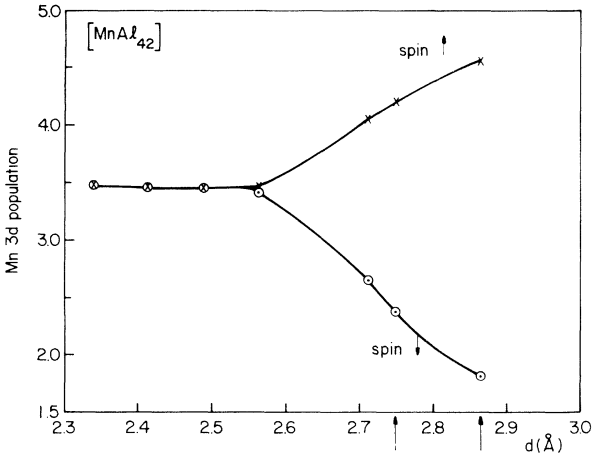

FIG. 4. Variation of 3*d* population with Mn-NN distance in $[MnAl_{42}]$. Arrows as in Fig. 2.

compression of the Mn-NN bond is produced by a decrease in the spin-up 3*d* population and simultaneous increase in the spin-down population, in such a way as to keep the total 3*d* population almost constant. However, in the case of *Al*Mn the spin-up and spin-down populations rapidly collapse to the same value and the moment is quenched.

We now turn our attention to the possible mechanisms underlying the observed magnetic behavior. In our previous calculations for *Al*Fe, we associated the instability of the magnetic moment of the Fe impurity to a large antiferromagnetic response of the host. The ratio μ(cluster)/μ(Fe) at the Al lattice distances was significantly smaller for *Al*Fe than for other systems with more stable magnetism, e.g., *Ca*Fe. With the present calculations, at the Mn-NN equilibrium distances, we obtained for the ratio μ(cluster)/μ(Mn) the values 0.74 for $[MnAl_{42}]$ and 0.96 for $[MnCu_{42}]$ (see Table I), which again demonstrates that local moments in Al induce a relatively larger antiferromagnetic response on the host neighbor atoms. This contributes to the instability of μ(Mn) and increases the sensitivity to local environment effects such as lattice compression.

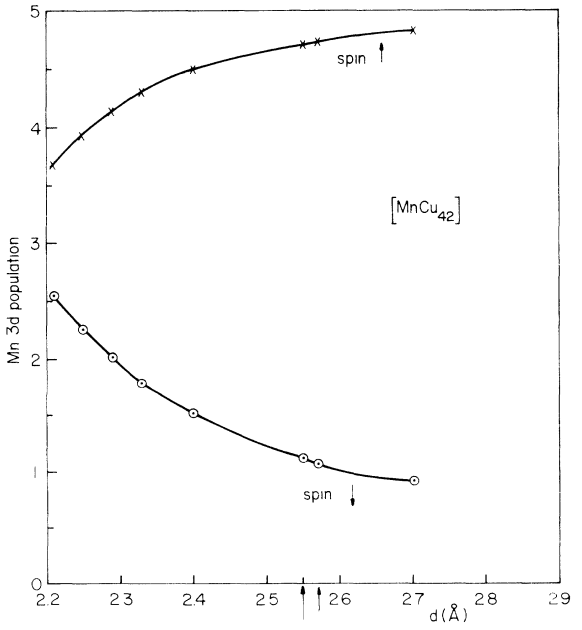

FIG. 5. Variation of 3*d* population with Mn-NN distance in $[MnCu_{42}]$. Arrows as in Fig. 3.

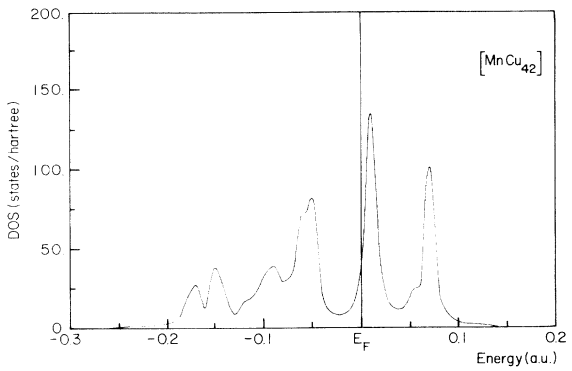

FIG. 6. 3*d* local density of states on Mn in $[MnCu_{42}]$ at *d*(Mn-NN)=2.57 Å.

Another factor that tends to produce large moments on Fe substitutional impurities in alkaline-earth-metal hosts such as Mg, Ca, and Sr is the very large lattice constants of the hosts, which, even taking into account relaxation, tends to isolate the impurity atoms and, suppressing hybridization, preserve atomiclike moments.[4] However, in the case of Cu the lattice constant is not larger, and so other mechanisms must play a role in preserving a large spin moment on Mn. We believe that the 3*d*(Mn)-3*d*(Cu) hybridization has an important effect. In fact, a comparison of the 3*d* local DOS on Mn (Fig. 6) with that on nearest-neighbor Cu (Fig. 7) shows that the 3*d* levels of Cu, as expected, occur at lower energy than Mn. The 3*d* DOS of Mn shows a structure at lower energies, which may thus be ascribed to hybridization with the Cu 3*d* orbitals. As a consequence, the 3*d* spin DOS (spin-up minus spin-down DOS) on Mn also presents a positive contribution at lower energies (see Fig. 8). This lower-energy "hard" part of the spin moment contributes to its stability and makes it less susceptible to environmental

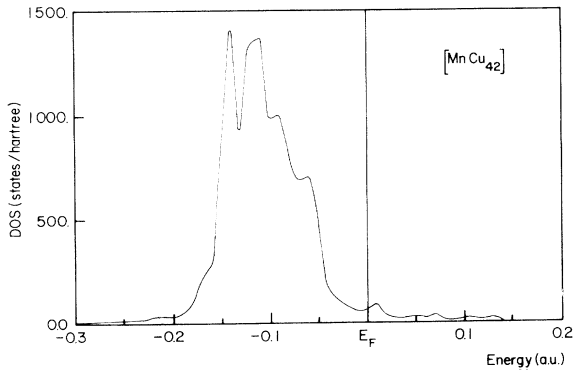

FIG. 7. 3*d* local density of states on Cu(NN) (12 atoms) in $[MnCu_{42}]$.

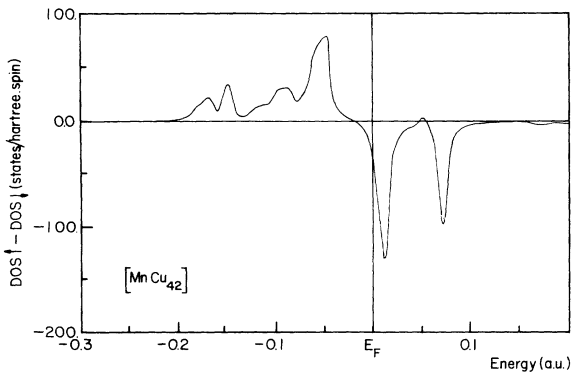

FIG. 8. 3*d* spin density of states (spin-up minus spin-down DOS) on Mn in $[MnCu_{42}]$.

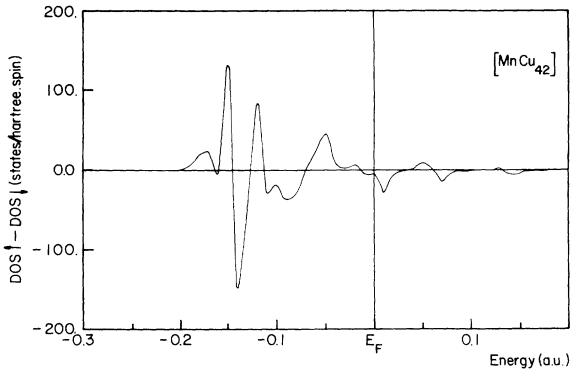

FIG. 10. 3*d* spin density of states on the 12 Cu(NN) in $[MnCu_{42}]$.

effects, which affect mostly electrons near the Fermi level. In contrast, the Mn 3*d* spin DOS in $[MnAl_{42}]$ shows mainly a narrow peak near the Fermi level (Fig. 9).

Examination of the 3*d* spin DOS on NN Cu (Fig. 10) reveals the lower-energy occupied spin-up and spin-down peaks of Cu and a structure near the Fermi level, induced by hybridization with Mn and responsible for the small 3*d* moment calculated on Cu.

To clarify further the differences in bonding in *Al*Mn and *Cu*Mn, we have plotted the bond-order energy distribution for the Mn-Al(NN) bond (Fig. 11) and Mn-Cu(NN) bond (Fig. 12). The bond order is the sum over occupied levels of the nondiagonal elements of the charge matrix, pertaining to a pair of atoms,[31] and may be directly related to the bonding strength. Positive bond orders are related to strong (bonding) bonds and negative to repulsive (antibonding) interactions. In Fig. 11 it may be seen that the Mn-Al(NN) bond-order energy distribution[32] shows a bonding peak near the Fermi level, the antibonding levels being unoccupied. In contrast, the Mn-Cu(NN) bond-order distribution shows a bonding region at lower energies, coincident with the lower-energy structure of the spin DOS, and an occupied antibonding region at higher energies near the Fermi level. This confirms our analysis of the magnetic moment on Mn.

IV. ORIGIN OF THE 3*s* SPLITTING IN XPS

A splitting of 2.9 eV observed in the Mn 3*s* level by XPS was interpreted as evidence of a magnetic moment of approximately $2.2\mu_B$ (Ref. 12) in *Al*Mn, in analogy with splittings seen in insulators such as MnF_2 and $MnCl_2$.[33] If we denote the relevant Mn spin occupation numbers as $3s(mm')$ and $3d(nn')$ briefly as $|mm'nn'\rangle$, where $m(n)$ is the number of spin-up electrons in orbital $3s(3d)$ and $m'(n')$ the number of spin-down electrons, then the ground-state configuration may be taken as $|G\rangle = |11nn'\rangle$, with $n > n'$, and the final ionic configurations as $|F1\rangle = |10ff'\rangle$ and $|F2\rangle = |01gg'\rangle$. If there is no large rearrangement of the 3*d* shell (or other spectator electrons), we can consider that $|F1\rangle$ will lie lower in energy than $|F2\rangle$ due to the larger exchange interaction of the remaining *s* electron with the majority-spin *d* electrons. On the other hand, even in insulators, XPS spectra of transition-metal *L* shells show a rich satellite structure, which is generally interpreted in terms of charge transfer and other relaxation processes sufficiently rapid to influence photoelectron energies.

In insulators, the metal $3s^k3p^63d^l$ configuration may display a well-defined multiplet structure. However, in

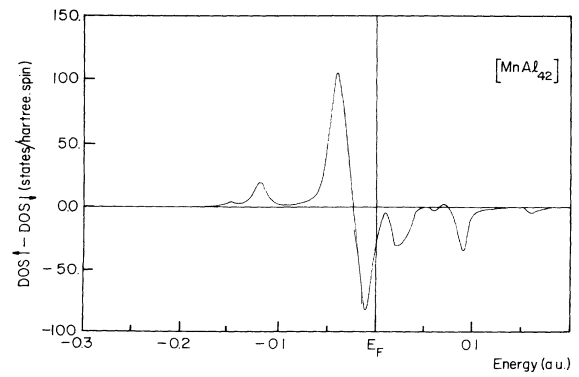

FIG. 9. 3*d* spin density of states on Mn in $[MnAl_{42}]$ at d(Mn-NN) = 2.75 Å.

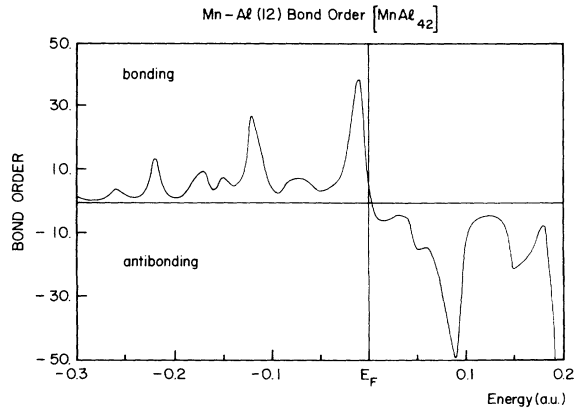

FIG. 11. Bond-order energy distribution in $[MnAl_{42}]$ for the 12 Mn-Al(NN) bonds.

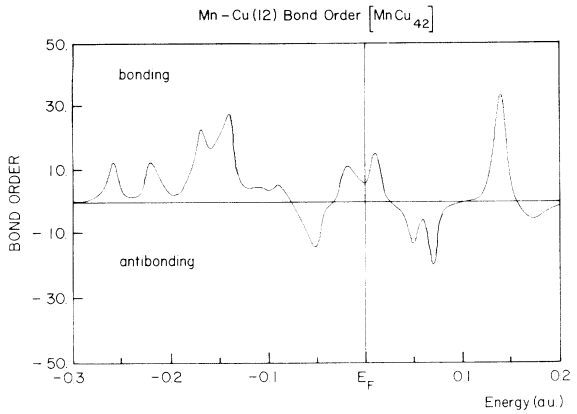

FIG. 12. Bond-order energy distribution in $[MnCu_{42}]$ for the 12 Mn-Cu(NN) bonds.

metallic hosts such as Al and Cu, the Mn $3d$ levels are strongly hybridized with neighboring atom states, and a simplified analysis in terms of one-, two-, and many-electron excitations in the Fermi-Dirac model is appropriate. In this environment we may expect rapid relaxation to occur around the Mn core hole, and so a more detailed investigation is needed. In fact, we find that even if the Mn-Al nearest-neighbor distance is compressed such that the ground-state moment is completely suppressed, the core hole is capable of inducing a transient $3d$ moment. In such a case, it is possible that the XPS reflects an excited-state moment, rather than the ground-state moment of the impurity. To display these effects, we show in Table II the results for $3s$ levels in the ground state (GS), transition state (TS), and ionic state (IS). In each case the numerical atomic basis on Mn was optimized in the appropriate $3s^k$ configuration, since the core-hole potential produces both direct energy-level shifts and indirect exchange effects through orbital contraction.

As can be seen from Table II, the exchange splitting $\Delta\varepsilon$ of the $3s$ level in the ground state at the equilibrium Mn-Al(NN) distance is ~ 1.4 eV, considerably less than the splitting observed in the experiment. However, comparison of the one-electron $3s$-level splitting to experiment is not an accurate procedure, since the latter expresses the difference in energy between states of different spin multiplicity produced by ionization of a $3s\uparrow$ and a $3s\downarrow$ electron, and $\Delta\varepsilon$ is a property of the ground state. Moreover, relaxation of the remaining electrons following the ionization of a core electron may be considered to be important and will be different for $3s$ spin up and spin down.

In Table II we show the result of the ionization energy from the $3s\downarrow$ level as obtained by a TS calculation.[34] In such a procedure, a SCF calculation is performed for a configuration in which $\frac{1}{2}$ electron is removed from the orbital; the resulting one-electron eigenvalue may be compared to the ionization energy, i.e., total-energy difference, with relaxation effects included to second order in occupation number. It may be observed that the $3s\downarrow$ ionization energy obtained in this manner compares better with experiment than the one-electron level energy in the ground state. It would be desirable to apply the same procedure to the $3s\uparrow$ level; however, this was not possible since, during the SCF iterations, the first transition state was recovered, since it has the most stable (Hund's rule) spin arrangement of parallel $3s$ and $3d$ moments. For the same reason, no convergence was obtainable for the ionized $3s(0\,1)3d(nn')$ configuration $(n > n')$.

In the $(mm')=(1\,\frac{1}{2})$ TS calculation, the excitation energy ε' is in good agreement with the low-ionization-energy experimental peak. Although it has no fundamental significance, we note that the nonoptimized majority-spin energy ε is also in good agreement with the high-ionization-energy XPS peak (Table II). Furthermore, noting the sequence of $3s$ splittings $\Delta\varepsilon$ (GS < TS < IS) and moments $\mu(3d)$:GS < TS $\simeq$ IS, we can see that the $3s$ and $3d$ shells are tightly coupled through the exchange interaction. Opening the $3s$ shell has several effects.

(1) Exchange coupling occurs between $3s$ and $3d$ shells, which stabilizes the majority spin of both shells.

(2) The core hole leads to contraction of radial functions, increasing the exchange energy and splittings.

(3) In an effort to shield the core hole, Mn draws electrons from the host, primarily filling the $3d\downarrow$ levels, and thus tending to reduce the moment.

In the TS we can see that effect (2) dominates over (3), while the $3s$ hole of the IS attracts sufficient charge $(0.65e)$ to begin to reduce the moment.

Ionization from the $3s\downarrow$ level (Table II) at the experimentally determined Mn-Al(NN) distance produces a $3d$ magnetic moment of $2.24\mu_B$, significantly larger than the

TABLE II. Energies (in eV) of $3s(mm')$ levels of Mn in *Al*Mn. m is the number of spin-up electrons in the $3s$ orbital, m' is the number of spin-down electrons, ε is $3s$ spin-up level energy, and ε' is $3s$ spin-down energy. GS=ground state, TS=transition state, IS=ionized state, and IS*=ionized state for Mn-Al distance =2.49 Å, at which point the ground-state moment is completely quenched.

	m	m'	ε	ε'	$\Delta\varepsilon$	$\mu(3d)$ on Mn	Charge on Mn
GS	1	1	82.11	80.73	1.38	1.82	−0.40
TS	1	$\frac{1}{2}$	84.57	81.69	2.88	2.32	−0.04
IS	1	0	86.44	82.99	3.45	2.24	+0.25
IS*	1	0	86.02	82.98	3.04	1.46	−0.14
Experiment[a]			~85	~82	2.9		

[a]From Ref. 12.

ground-state moment. This indicates the existence of complex nonlinear effects due to the interaction between the $3d$ and $3s$ moments. Indeed, a calculation for the ionized configuration, at a Mn-Al(NN) distance for which μ(Mn) is zero in the ground state (see Fig. 2), gave $\mu(3d)=1.46\mu_B$, a direct evidence of the strong polarization of the $3d$ shell induced by the $3s\uparrow$ electron left in the core. Thus we conclude that the existence of a $3s$ exchange splitting in the XPS spectrum may not be taken as evidence of a magnetic moment on the impurity in the ground state.

V. CONCLUSIONS

Employing 43-atom embedded SFC cluster calculations in the framework of local spin-density theory, we have calculated the electronic structure of a Mn impurity in Al and Cu hosts. Spin magnetic moments on Mn of $2.91\mu_B$ in Al and $3.81\mu_B$ in Cu were found for calculations performed at the unperturbed host lattice interatomic distances. Investigation of the effect of displacement of the first shell of host atoms around the impurity on its magnetic moment revealed that Mn in Al is much more sensitive to compression than Mn in Cu. Calculated moments at the Mn nearest-neighbor interatomic distances as determined by XAFS measurements[28] gave $1.92\mu_B$ for Mn in Al and $3.88\mu_B$ for Mn in Cu. Analysis of the mechanisms of the environment effects on μ showed that the larger antiferromagnetic response of the host around Mn in Al is important in explaining the observed sensitivity to relaxation. Furthermore, Mn in Cu has its moment stabilized by hybridization of the $3d$ orbitals of Mn with the $3d$ of the neighbor Cu atoms.

Calculations for the configuration obtained by ionizing one electron from the $3s$ shell of Mn lead to the conclusion that the $3s$ exchange splitting observed in XPS spectra[12] may not be taken as evidence of a $3d$ moment in the ground state. In fact, even for a calculation at a Mn-NN distance for which the moment is completely quenched in the ground state, a large ($\sim 1.5\mu_B$) $3d$ moment is present at the ionized configuration, due to $3d$ polarization by the $3s$ electron left in the core.

ACKNOWLEDGMENTS

Calculations were performed at the NERSC Cray YMP of Lawrence Livermore National Laboratory. This work was supported by the National Science Foundation, through the U.S.-Brazil cooperative program, by the U.S. Department of Energy, Grant No. DE-FG02-84ER45097, and by the Conselho Nacional de Desenvolvimento Cientifíco e Tecnológico (CNPq). D.G. thanks P. H. Dederichs for calling attention to the XAFS measurements.

[1]C. Rizzuto, Rep. Prog. Phys. **37**, 147 (1974).
[2]G. Grüner, Adv. Phys. **23**, 941 (1974).
[3]D. Guenzburger and D. E. Ellis, Phys. Rev. Lett. **67**, 3832 (1991).
[4]D. Guenzburger and D. E. Ellis, Phys. Rev. B **45**, 285 (1992).
[5]K. H. Fischer, in *Kondo and Spin-Fluctuation Systems,* edited by K. H. Hellwege, Landolt-Börnstein, New Series, Group III, Vol. 15 (Springer-Verlag, Berlin, 1982).
[6]C. M. Hurd, J. Phys. Chem. Solids **30**, 539 (1969).
[7]D. Riegel and K. D. Gross, Physica B **163**, 678 (1990).
[8]L. Moberly, T. S. Steelhammer, O. G. Symko, and W. Weyhmann, J. Low Temp. Phys. **33**, 21 (1978).
[9]C. P. Flynn, D. A. Rigney, and J. A. Gardner, Philos. Mag. **15**, 1255 (1967).
[10]G. Bauer and E. Seitz, Solid State Commun. **11**, 179 (1972).
[11]N. Kroó and Z. Szentirmay, Phys. Rev. B **10**, 278 (1974).
[12]P. Steiner, H. Höchst, W. Steffen, and S. Hüfner, Z. Phys. B **38**, 191 (1980).
[13]D. E. Ellis, Int. J. Quantum Chem. Suppl. **2**, 35 (1968); D. E. Ellis and G. S. Painter, Phys. Rev. B **2**, 2887 (1970).
[14]See, for example, R. G. Parr and W. Yang, *Density-Functional Theory of Atoms and Molecules* (Oxford University Press, New York, 1989).
[15]A. Rósen, D. E. Ellis, H. Adachi, and F. W. Averill, J. Chem. Phys. **65**, 3629 (1976).
[16]U. von Barth and L. Hedin, J. Phys. C **5**, 1629 (1972).
[17]D. E. Ellis, G. A. Benesch, and E. Byrom, Phys. Rev. B **16**, 3308 (1977).
[18]R. S. Mulliken, J. Chem. Phys. **46**, 497 (1949).
[19]B. Delley and D. E. Ellis, J. Chem. Phys. **76**, 1949 (1982).
[20]D. Bagayoko, N. Brener, D. Kanhere, and J. Callaway, Phys. Rev. B **36**, 9263 (1987).
[21]R. M. Nieminen and M. Puska, J. Phys. F **10**, L123 (1980).
[22]J. Deutz, P. H. Dederichs, and R. Zeller, J. Phys. F **11**, 1787 (1981).
[23]P. J. Braspenning, R. Zeller, A. Lodder, and P. H. Dederichs, Phys. Rev. B **29**, 703 (1984).
[24]Y. Jinlong, L. Huibin, W. Kelin, L. F. Donà dalle Rose, and F. Toigo, Phys. Rev. B **44**, 10 508 (1991).
[25]N. Stefanou, P. J. Braspenning, R. Zeller, and P. H. Dederichs, Phys. Rev. B **36**, 6372 (1987).
[26]H. J. F. Jansen, K. B. Hathaway, and A. J. Freeman, Phys. Rev. B **30**, 6177 (1984).
[27]M. Sigalas, D. A. Papaconstantopoulos, and N. C. Bacalis, Phys. Rev. B **45**, 5777 (1992).
[28]U. Scheuer and B. Lengeler, Phys. Rev. B **44**, 9883 (1991).
[29]J. R. Davis and T. J. Hicks, J. Phys. F **9**, 753 (1979).
[30]R. J. Higgins and R. H. Hendel, Solid State Commun. **39**, 47 (1981).
[31]A. Szabo, *Modern Quantum Chemistry* (Macmillan, New York, 1982).
[32]R. Hoffmann, *Solids and Surfaces: A Chemist's View of Bonding in Extended Structures* (VCH, New York, 1988).
[33]B. W. Veal, D. E. Ellis, and D. J. Lam, Phys. Rev. B **32**, 5391 (1985), and references therein.
[34]J. C. Slater, *The Self-Consistent Field for Molecules and Solids* (McGraw-Hill, New York, 1974), Vol. 4.

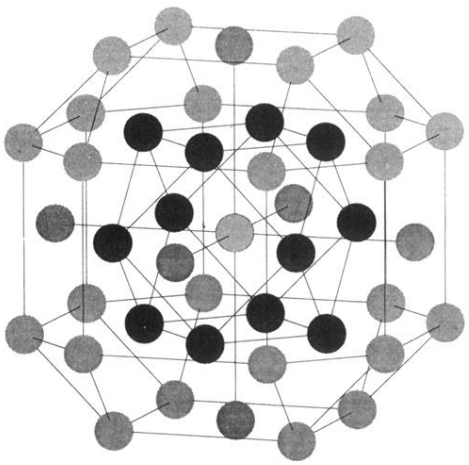

FIG. 1. View of the 43-atom cluster representing a Mn impurity in fcc Al and Cu. Darker spheres are atoms in the first shell of neighbors surrounding the central Mn.